ORIGINAL PAPER

CrossMark

Nanostructured aptamer-based sensing platform for highly sensitive recognition of myoglobin

Neda Ghafori Nia[1] · Azadeh Azadbakht[1]

Abstract
A composite was prepared from PtSn nanoparticles and carbon nanotubes (PtSnNP/CNTs) and applied to the electrochemical determination of myoglobin (Mb). An Mb-aptamer was immobilized on a glassy carbon electrode (GCE), and hexcyanoferrate was used as an electrochemical probe. The PtSnNP/CNTs were synthesized by a microwave-aided ethylene glycol reduction method. Detection is based on electron transfer inhibition that is caused by the folding and conformational change of the Mb-aptamer in the presence of Mb. The amperometric signal for hexacyanoferrate, best measured at 0.2 V vs. Ag/AgCl depends on the concentration of Mb that interacts with the aptamer on the GCE. This approach is selective and sensitive for Mb due to (a) the highly specific recognition ability of the aptamer for Mb, (b) the powerful electronic properties of carbon nanotubes, (c) the arranged decoration of CNTs with PtSnNPs, and (d), the superior electron transfer to hexacyanoferrate. The assay is highly selective, with linear relationships from 0.01–1 nM and 10 nM–200 nM, and a limit of detection as low as 2.2 ± 0.1 pM. The modified GCE was applied to the quantitation of Mb in spiked human serum samples.

Keywords Aptasensor · PtSn nanoparticles · Microwave-aided reduction · Carbon nanotubes

Introduction

Acute myocardial infarction (AMI), also known as heart attack, is the main cause of morbidity and mortality worldwide [1]. More than 30% of adult deaths in the 30–70 year age group (greater than the mortality rate from all types of cancer) have been caused by cardiovascular diseases [2]. Therefore, cardiac pathology diagnosis has received utmost attention. Up until now, various cardiac biomarkers have been reported due to their prime role in the early diagnosis of AMI [3]. Among the different cardiac biomarkers, myoglobin (Mb) has been widely recognized as one of the best candidate markers because its elevated level indicates myocardial damage [4, 5]. Also, it has become a gold standard diagnosis of patients with acute myocardial infarction as it is permeated in the biological

fluids (urine and blood stream) within 4–5 h after an AMI episode [6]. In AMI, the Mb concentration can increase up to 600 ng/mL compared to its normal range (6–100 ng/mL) [7, 8]. Mb is a single-chain protein containing 153 amino acids and heme (iron-containing porphyrin) group in the center. This protein as a constituent element in the muscle tissue of vertebrates in general and in almost all mammals plays an important role as an oxygen store in muscle tissue [9]. At present, various approaches have been reported for Mb quantification including mass spectrometry [10], liquid chromatography [11], luminescence [12], colorimetric [13], and surface plasmon resonance (SPR) [14]. But most of these methods rely on analysis in centralized laboratories which are often costly and time-consuming. Thus, development of simple method to detect Mb at the point of care (POC) based on biochemical assays have been considered as an essential need [15].

Since the first discovery in 1990s [16] molecular probes based on nucleic acid (aptamer) platforms as supplement to antibody-based methods have revealed significant consideration in the fields of diagnostics, and therapeutics [17]. Nucleic acid aptamers which are often called chemical antibodies have been employed as comparable or superior alternatives to antibodies due to their unique properties in terms of small size, high binding affinity for variety kind of molecules

✉ Azadeh Azadbakht
Azadbakht.a@gmail.com; Azadbakht@khoiau.ac.ir

[1] Department of Chemistry, Khorramabad Branch, Islamic Azad University, Khorramabad, Iran

(nucleic acids, proteins, cells and even tissues), molecular flexibility, in vitro screening, and ease of chemical modification [18]. The combination of highly specific recognition ability of nucleic acid aptamers with considerable properties of nanomaterials offer the possibility of creating the novel diagnostic platforms with enhanced selectivity and unprecedented sensitivity compared with available conventional detection methods [19]. Among different nanomaterials, carbon nanotubes (CNTs) have become promising candidate for design and fabrication of biosensors due to their unique electronic properties [20, 21].

The effective screening of Mb with high affinity based on employing Mb-aptamer as molecular recognition element has been considered. CNTs supported PtSn nanoparticle as a sensing platform was prepared by intermittent microwave-assisted ethylene glycol reduction method. The PtSnNP/CNTs and Mb-aptamer was immobilized at the surface of GCE through the drop casting and covalent amide bonds, respectively. The use of PtSnNP/CNTs led to electrochemical signal amplification due to synergistic effects of the nanocomponent materials. By adding Mb molecule as a target, the Mb/aptamer complex was formed on the surface and the electron transfer characteristic of $[Fe (CN)_6]^{3-/4-}$ as a probe was changed.

Experimental

Chemicals

All the chemical materials employed in this paper were of analytical grade. Multi-walled carbon nanotubes with 95% purity and 1 mm length were obtained from Nanolab (Brighton, www.nano-lab.com). Hexachloroplatinate (IV) hydrate (H_2PtCl_6-$5H_2O$), stannous chloride dehydrate ($SnCl_2$. $2H_2O$), ethylene glycol (EG), isopropyl alcohol (99.5%), nitric acid (HNO_3, 60%), sulfuric acid (H_2SO_4, 97%), sodium hydroxide (NaOH, 98%,), nafion solution (5% in water/alcohol mixture) were purchased from Merck (Germany, http://www.merck.com/index.html).1-Ethyl- 3-(3-dimethylaminopropyl) carbodiimide hydrochloride (EDC) was prepared from Sigma-Aldrich (http://www.sigmaaldrich.com/european-export.html). All aqueous solutions were prepared with double-distilled water. The Mb-binding aptamer (NH_2-$(CH_2)_6$ CCC TCC TTT CCT TCG ACG TAG ATC TGC TGC GTT GTT CCGA) was synthesized and purified from Bioneer (South Korea, http://www.bioneer.com). Phosphate buffer was used as working buffer throughout the experiment containing 0.1 M Na_2HPO_4, 0.1 M KH_2PO_4 and 0.5 M NaCl. All experiments were performed at ambient temperature of 25 ± 1 °C.

Instruments and apparatus

All electrochemical measurements including cyclic voltammetry (CV), differential pulse voltammetry (DPV) and electrochemical impedance spectroscopy (EIS) were carried out using a computer controlled Autolab potentiostat/galvanostat (PGSTAT204, Eco-Chemie, The Netherlands; https://www.metrohm.com/en). All CVs measurement were performed in the presence of 10 mL $K_3[Fe(CN)_6]$/$K_4[Fe(CN)_6]$ (1:1) 5.0 mM and 0.1 M phosphate buffer (pH = 7.4) by sweeping the potential between −0.6 V and 0.8 V at 50 mV s^{-1}. All EIS response were obtained in 10 mL phosphate buffer 0.1 M and 5.0 mM $K_3[Fe(CN)_6]$/$K_4[Fe(CN)_6]$ (1:1) solution in the frequency range from 0.1 Hz and 10 kHz with 5 mV as signal amplitude and 0.2 V bias potential. All DPV signals were recorded in 10 mL phosphate buffer 0.1 M and 5.0 mM $K_3[Fe(CN)_6]$/$K_4[Fe(CN)_6]$ (1:1) with a modulation amplitude of 0.05 V, a pulse width of 0.05 s, step potential of 0.001 mV, and sample width of 0.0167 s. The NOVA 1.8 and Frequency Response Analyzer (FRA) software was employed for data analysis. A three electrode system including a modified and unmodified GCE as a working electrode, a saturated Ag/AgCl electrode as a reference electrode and a platinum wire as a counter electrode were used. Morphology and size of the particles was monitored using scanning electron microscopy (SEM), taken by an X-30 Philips instrument. Also, the energy-dispersive X-ray (EDS) and wavelength-dispersive X-ray (WDX) spectroscopy were carried out by a Vega-Tescan electron microscope.

Preparation of PtSnNP/CNTs nanocomposite

Oxidation treatment of nanotubes were carried out by refluxing CNTs in concentrated HNO_3 and H_2SO_4 for 12 h at a temperature of 150 °C in order to purify the CNTs and introduce some oxygen-containing groups on the carbon surface. Afterward, the solids were washed with double deionized water, filtered, and dried at a temperature of 60 °C. After repetition this process several times, the sediment was sonicated in the solution containing HNO_3 and H_2SO_4 (1:3, v/v) for 3 h, while the pH of the suspension was adjusted to 8.0 using NaOH (15%). In the last step, the resultant CNTs were centrifuged and dried subsequently until the functionalized carbon nanotubes were achieved. PtSnNP/CNTs nanocomposite was synthesized according to the method reported by Chen et al. [22] (All details and explanations are described in Electronic Supporting Material (ESM). In this protocol, ethylene glycol was quickly warmed up and oxidized to aldehydes, glycolic acid, carboxylic acids, and CO_2, causing the reduction of Pt and Sn metal ions [23]. The protonated form of glycolic acid in an acidic media plays an essential role as stabilizer for metal colloids through forming the chelate-type

complexes via their carboxylic groups and the surrounding the metal nanoparticles [22].

Electrode modification

For construction of PtNP/CNT/GCE, the bare GCE was polished carefully with 0.3, 0.1 and 0.05 μm alumina powder and then cleaned thoroughly using an ultrasonic bath in 1: 20 (*v*/v) nitric acid and ethanol solution. PtSnNP/CNTs nanocomposite was prepared as follows: 5 mg of PtSnNP/CNTs nanocomposite, 100 mL of nafion solution (5 wt% in ethanol) and 1 mL of isopropyl alcohol were mixed by sonication to form a homogeneous composite. Then 10 μL of the synthesized composite was placed on a GCE. Afterwards, the modified electrode was washed with phosphate buffer.

Preparation of aptamer/PtSnNP/CNT/GCE

Amine functionalized Mb-aptamer at 100 μM was mixed with EDC at 100 mM in phosphate buffer. Mb-aptamer immobilization was performed by incubation 10 μL amine functionalized Mb-aptamer onto the surface of the modified electrode. The covalent attachment of the amine functionalized Mb-aptamer onto the PtSnNP/CNT/GCE surface took place via the formation of a favored amide bond between the NH_2 group of the amine-terminated Mb-aptamer and the carboxyl groups on the nanotubes. Afterwards, the modified electrode (denoted aptamer/PtSnNP/CNT/GCE) was rinsed with phosphate buffer to eliminate the unbounded substrate and used for the electrochemical experiments.

Mb quantitation using electrochemical measurement

In order to evaluate the performance of aptasensor, modified electrode was incubated in the solution containing Mb as a target molecule. Mb target binding at the surface of aptasensor induced folding and conformational change in the aptamer structure. In fact, due to the formation of aptamer/Mb complex the electron transfer of the redox probe was prevented from the electrode surface, resulting in the decrease of DPV anodic peak current. The decreased current intensity was monitored as a function of the Mb concentration. Figure 1 depicts the mechanism of this strategy in the construction of the electrochemical aptasensor for Mb detection.

Results and discussion

Choice of materials

This study reports the design and evaluation of a new synthetic receptor assay for Mb recognition. Determination of Mb was performed by amalgamation the unique feature of Mb-aptamer as a biomolecular recognition elements and wonderful property of CNTs supported PtSnNPs for amplification the electrochemical signal. It has been reported that PtSnNPs prepared by microwave-assisted method showed the most satisfied distribution on CNTs surface leading to increased surface area [22]. In addition to electrochemical signal improvement, PtSnNP/CNTs play an important role for aptamers attachment. Abundant carboxyl groups in CNTs makes this platform as significant transduction to prepare aptasensor by allowing Mb-aptamer immobilization by covalent amide bonds formed between the carboxyl groups on the nanotubes and the amino groups on the oligonucleotides. Owing to the large surface area, good physical tubular structure, high surface-to-volume ratio, strong adsorptive ability and numerous carboxyl groups in platform, huge amount of aptamers are captured on PtSnNP/CNTs interface and amplified electrochemical response is expected. The superb electron transition of $[Fe(CN)_6]^{3-/4-}$ as a redox probe, high affinity and specificity of diagnosis element, and integrated properties of individual nanomaterials in platform cause lower detection limit and wider linear range for aptasensor.

Characterization of modified electrode

Since the electrochemical applicability of modified electrode strongly depended on the composition, loading amount, distribution and size of nanocomposite, the morphology of the PtSnNP/CNTs and aptamer/PtSnNP/CNTs were investigated by using scanning electron microscopy (SEM), energy-dispersive X-ray (EDS) and Wavelength-dispersive X-ray (WDX). Figure 2a depicts the surface morphology of the bare GCE (A), CNT/GCE (B) PtSnNP/CNT/GCE (C) and aptamer/PtSnNP/CNT/GCE (D). As illustrated, CNTs are interwoven to give a network structure with the average diameter of about 50 nm. PtSnNP/CNTs nanocomposite indicates the satisfied distribution of PtSn nanoparticles on CNTs sidewall, except for a slight particle agglomeration (Fig. 2c). As evidenced from Fig. 2d, after attachment of Mb-aptamer, the morphology of the electrode surface is obviously changed, confirming aptamer immobilization to the surface. The EDS gives evidences for presence of the Pt, Sn, C, and O in the nanocomposite (Fig. S1A). Furthermore, based on the EDS spectra analysis, in the CNTs–COOH, the main elements is C with weight percent (wt%) of 81.52%, while in PtSnNP/CNTs–COOH, C, O, Sn, and Pt with the weight percent (wt%) of 68.45%, 20.58%, 7.32%, and 3.66% are presented, respectively. Further evidence for present the Sn, Pt elements in nanocomposite is obtained using WDX analysis. WDX images represent the distribution of C, O, Sn, and Pt (Fig. S1B-S1E, respectively).
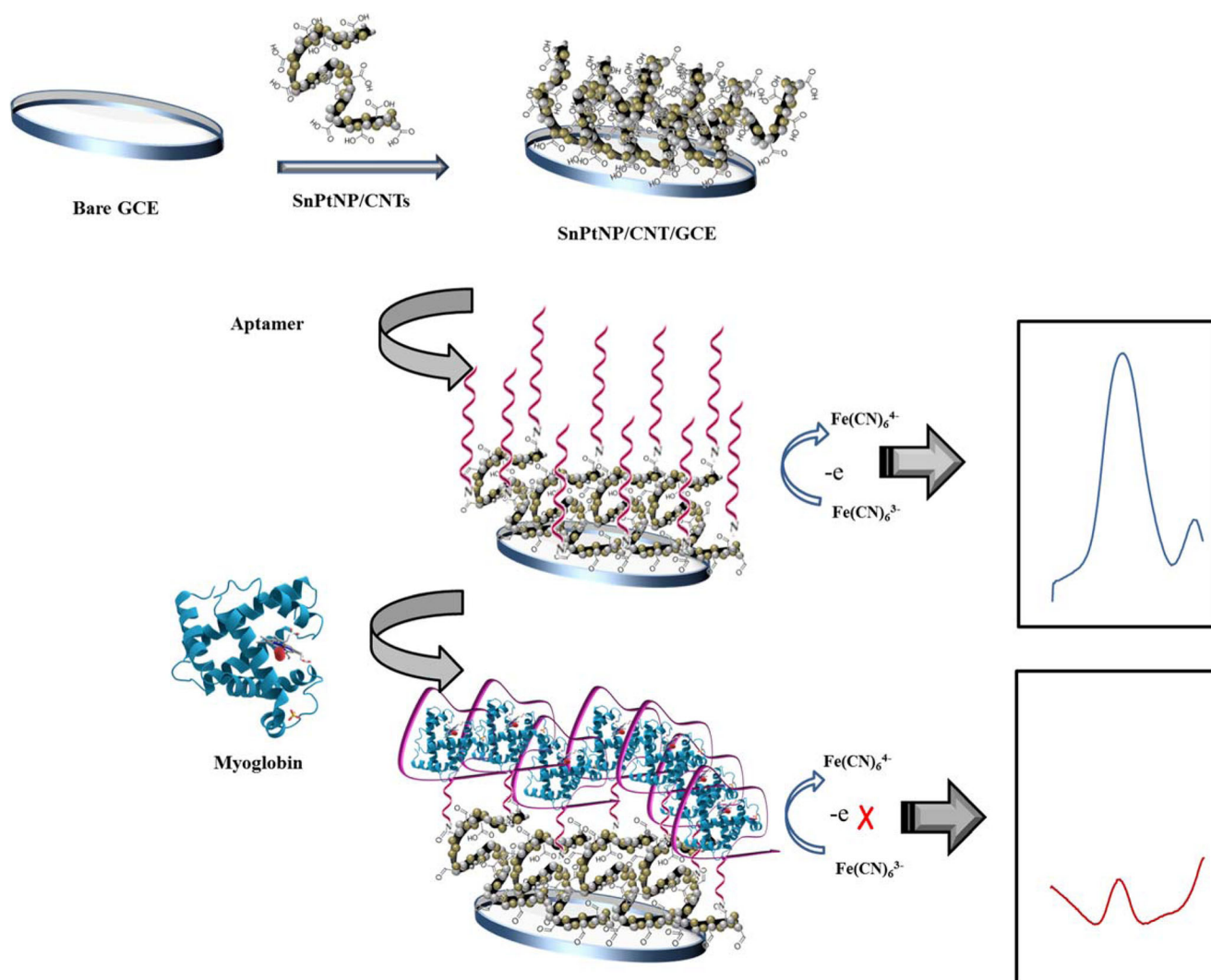
Fig. 1 Schematic representation for different steps of aptasensor fabrication

Optimization of method

The optimization of the experimental condition considered as the first step of the experiment design. For this goal, some important parameters such as concentration of Mb-aptamer and incubation time of Mb were optimized. Based on our results, the best performance of aptasensor was achieved in 0.5 μM aptamer concentrations. Also, the optimum Mb incubation time were found to be 30 min (All required details, Fig.s (fig.S2 and Fig. S3) and explanation are presented in Electronic Supporting Material).

Electrochemical behavior of aptasensor

In order to characterize the fabrication processes of the aptasensor, CVs method was employed and the curves of different modified electrodes conducted in the solution containing 5.0 mM $[Fe(CN)_6]^{3-/4-}$ and 0.1 M phosphate buffer with a scan rate of 50 mVs^{-1} were recorded. The

CVs response of bare GCE (curve a), CNT/GCE (curve b), PtSnNP/CNT/GCE (curve c), aptamer/PtSnNP/CNT/GCE (curve d), and Mb/aptamer/PtSnNP/CNT/GCE (curve e) lectrodes are shown in Fig. 3. As shown, remarkable changes in the CVs response are appeared upon the stepwise construction of the aptasensor. The GCE modified with CNTs show a significant increase in current response in comparison to the bare electrode (curve b). The enhanced electrochemical current of CNT/GCE is attributed to the fact that CNTs improves the conductivity of the electrode and facilitates the electron transfer of the redox probe. Based on Chen's report [22] small and well dispersed PtSnNP at the surface of CNT obtained when PtSnNP/CNT prepared by microwave-assisted ethylene glycol reduction method. This phenomenon causes enlarged active surface area of the electrode. Taking this explanation into account, the maximum redox peak current of PtSnNP/CNT/GCE can be ascribed to the high active surface area of the electrode (curve c).
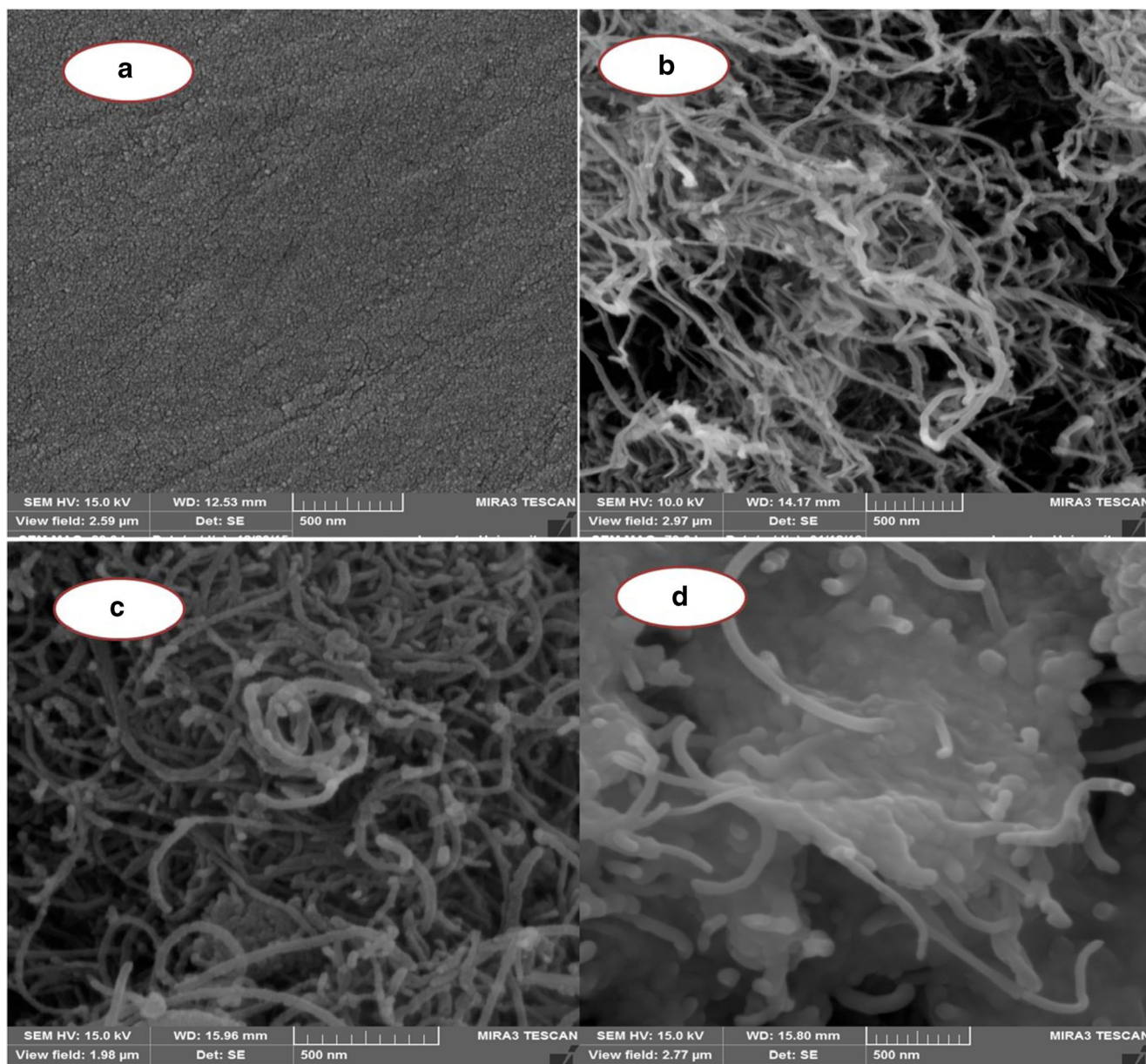
Fig. 2 Typical SEM image of bare GCE (**a**), CNT/GCE (**b**) PtSnNP/CNT/GCE (**b**) and aptamer/PtSnNP/CNT/GCE (**d**)

According to Fig. 3, for aptamer/PtSnNP/CNT/GCE the current value decrease (curve d), owing to electrostatic repulsive force between the negative charges of the aptamer phosphate groups and $[Fe(CN)_6]^{3-/4-}$ anions probe. As obviously can be seen, the extent of the electrode response is further decline by loading the target molecule onto the electrode surface (curve e). Since incubation of Mb on the electrode surface induce conformational change in the aptamer structure, the electron transfer of the redox probe is retarded from the electrode surface and even more decline in the peak response is obtained.

These observations were further supported by impedance measurements. The impedance spectra contain a semicircle and a linear segment. The semicircle segment at higher frequencies is associated with the electron transfer- limited-process, and the linear segment at lower frequencies is corresponds to the diffusion-limited process. The result of the change in the interfacial resistance R_{ct} (charge transfer resistance) is shown as the semicircle diameter changes, which is due to the electron transferring from the surface of the modified electrode to $[Fe(CN)_6]^{3-/4-}$ solution. Figure 4 shows EIS plots obtained at a potential of 0.2 V for bare GCE (curve a), CNT/GCE (curve b), PtSnNP/CNT/GCE (curve c), aptamer/PtSnNP/CNT/GCE (curve d), and Mb/aptamer/PtSnNP/CNT/GCE (curve e). The R_{ct} value of modified electrode increases in the order PtSnNP/CNT/GCE < CNT/GCE < bare GCE < aptamer/PtSnNP/CNT/GCE < Mb/aptamer/PtSnNP/CNT/GCE. The resultant EIS data corroborate the prior data
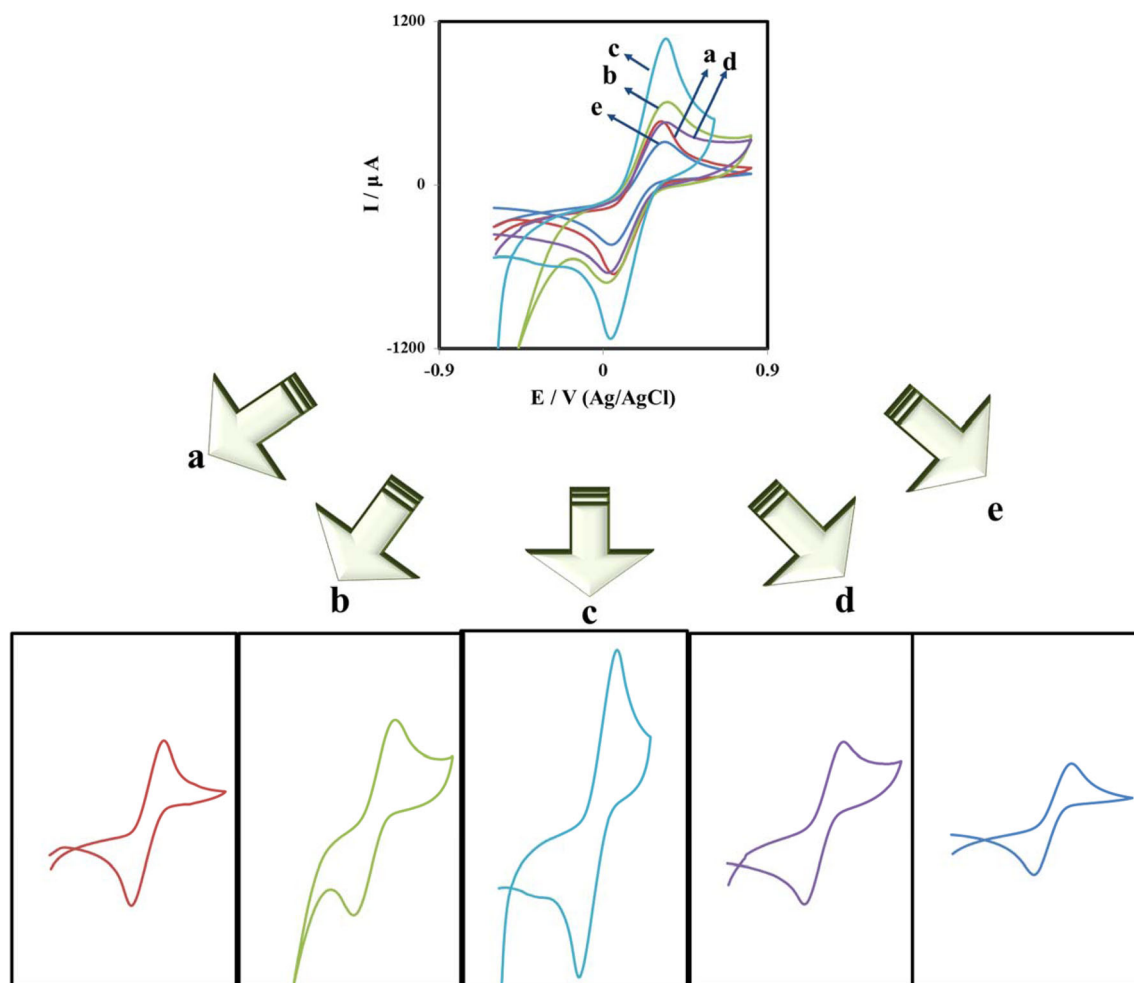
Fig. 3 CVs for bare GCE (curve a), CNT/GCE (curve b), PtSnNP/CNT/ GCE (curve c), aptamer/PtSnNP/CNT/GCE (curve d), and Mb/aptamer/ PtSnNP/CNT/GCE (curve e) recorded in the solution containing 5.0 mM $[Fe(CN)_6]^{3-/4-}$ and 0.1 M phosphate buffer. Condition: scan rate: 50 mV s^{-1}, sweeping potential: −0.6 V and 0.8 V

achieved by the CV, implying that the aptasensor fabrication was carried out successfully.

Electrochemical detection of Mb

To confirm applicability of our approach for Mb quantitation, Mb with different concentrations was measured in the cell media. Using an optimum condition, the calibration curves of modified electrode are exhibited in Fig. 5. The current intensity was monitored at a working voltage of 0.2 V vs. Ag/AgCl. When the concentration of Mb increased, the electrochemical signal of redox probe decreased accordingly. This phenomenon can be related to the electron transfer suppression due to folding and conformational change of Mb-aptamer oligonucleotides. The regression equation at low concentrations is (0.01–1 nM) I (μA) = −13.1 [Mb] (nM) + 116 with a correlation coefficient of 0.955 and a sensitivity of 185.7 μA. nM^{-1}. Cm^{-2}. For higher concentration range of Mb linear ranges is found from 10 nM–200 nM with the regression

equation of I (μA) = −0.288 [Mb] (nM) + 79.1 and correlation coefficient of 0.976. As shown in Fig. 5, when the concentration of Mb reaches 200 nM, the current intensity gradually level off. A higher Mb concentration produces only a small intensity variation. The detection limit (LOD) was experimentally determined to be 2.2 ± 0.1 pM based on a signal-to-noise ratio (S/N) of 3. As can be seen from Table 1, the overall performance of our assay (detection limit and linear range) as the function of the target concentration is much better in some cases or comparable with the other methods reported so far [24–35].

Real sample analysis

The practical applicability of the present method was examined on the assay of Mb in human serum sample. The serum samples were filtered using centrifugal filtration devices to remove macromolecules such as human serum albumin and other proteins such as globulin. The normal dosage range of
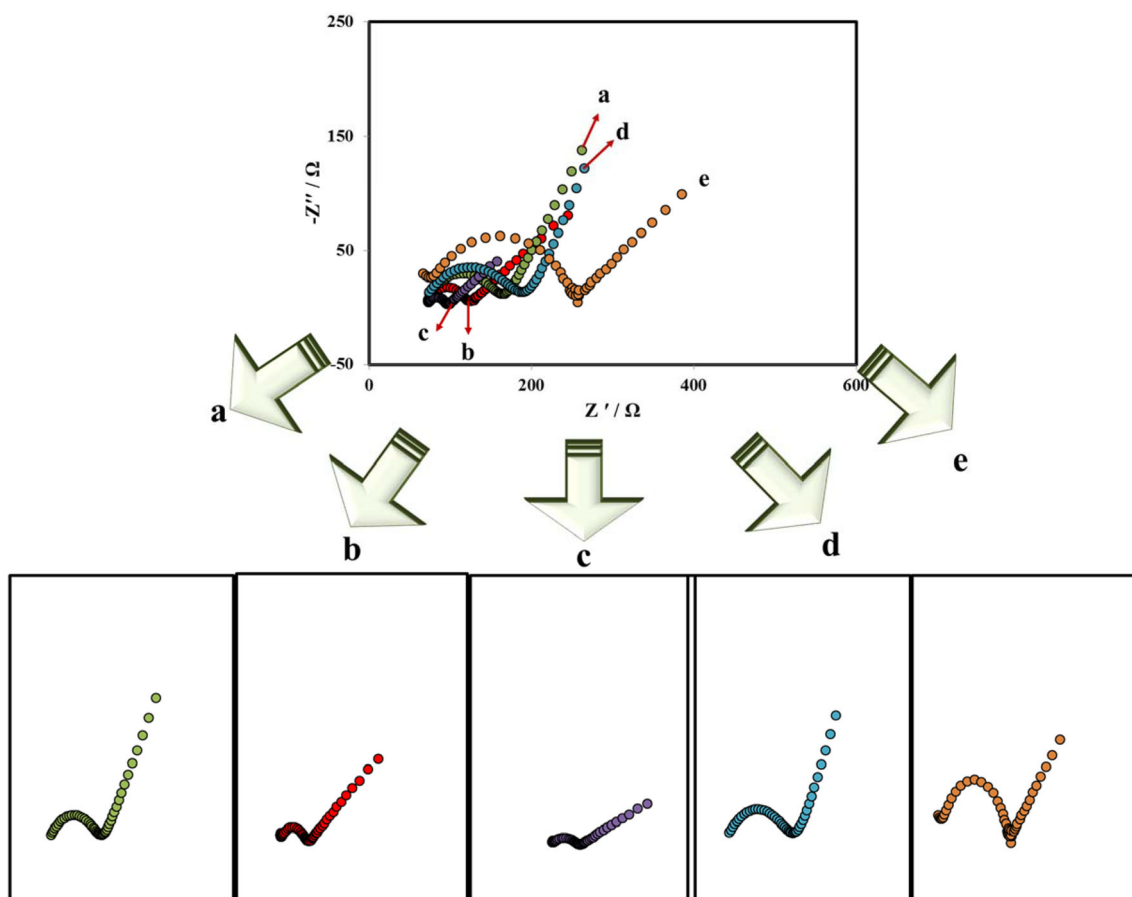
Fig. 4 Nyquist plots for bare GCE (curve a), CNT/GCE (curve b), PtSnNP/CNT/GCE (curve c), aptamer/PtSnNP/CNT/GCE (curve d), and Mb/aptamer/PtSnNP/CNT/GCE (curve e) recorded in the solution containing 5.0 mM $[Fe(CN)_6]^{3-/4-}$ and 0.1 M phosphate buffer. Condition: signal amplitude: 5 mV, frequency range: 10 kHz-0.1 Hz, bias potential: 0.2 V

Mb in human serum varied from 6 ng/mL (0.34 nM) to 100 ng/mL (5.6 nM) [7, 8]. In order to monitor Mb in human serum sample, the human serum samples were diluted 10 times using phosphate buffer. In the next step, three real samples were prepared separately by spiking known concentrations of Mb (3 nM, 5 nM, and 8 nM) into diluted serum samples. Then, the concentrations of Mb in the Mb-spiked serum were measured using the modified. All results are tabulated in Table S1. According to the results, Mb concentration recoveries of 94.4–98.3% with relative standard deviations between 1.4 and 3.5% are achieved; demonstrating aptasensor can be used to precisely determine Mb concentration in complex biological samples.

Specificity of the electrochemical aptasensor

The selectivity of the system for Mb detection in the presence of the interfering species was investigated by using different amounts of the interfering agent including hemoglobin, fructose, cytochrome c, and glucose. Based on the Fig. 6, even though, the interfering concentrations are 1000-fold higher than the Mb content, the variation of current responses by the addition of interferences are less than 10% of Mb signal, so no obvious interference for the determination of Mb was seen.

Stability of the aptasensor

The electrochemical stability of the aptasensor as an essential factor in practical experiments was checked by 50 repetitive potential sweep at a scan rate of the 50 mV s^{-1} in a 0.1 M phosphate buffer containing 5.0 mM $[Fe(CN)_6]^{3-/4-}$. As demonstrated in Fig. 7, after 50 repetitive sweep scans, the peak current intensity remains more or less intact, confirming that the electrochemical performance of the aptasensor is fairly stable, so that any removal of the aptamer from the surface of the electrode can be neglected.

The reproducibility of this analytical approach was also validated. For this goal, the current obtained of the three independent electrochemical aptasensors in the presence of 100 nM Mb were measured. The data revealed a relative standard deviation (RSD) of 6.7%, proving that the designed method was highly reproducible.

Fig. 5 DPV results for prepared aptasensor recorded in solution containing 5.0 mM $[Fe(CN)_6]^{3-/4-}$ and 0.1 M phosphate buffer after incubation with different concentration of Mb: 0, 0.01, 0.1, 1, 10, 50, 100 and 200 nM. **b** Plots of peak current vs. Mb concentrations. Condition: modulation amplitude: 0.05 V, pulse width: 0.05 s, sample width: 0.0167 s, step potential of 0.001 mV, working voltage: 0.2 V vs. Ag/AgCl
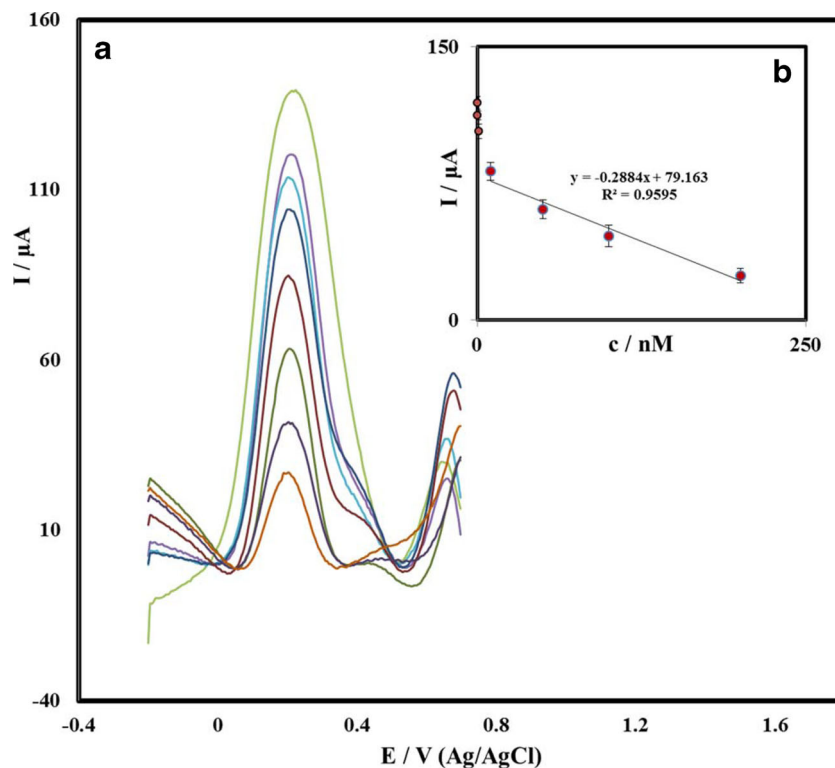
Conclusion

Our protocol is introduced based on using PtSnNP/CNTs nanocomposite as a signal amplifier and Mb-aptamer as a diagnosis element. Our nanocomposite simplified both the immobilization of the aptamer probe on its surface and the electron-transfer of the $Fe(CN)_6]^{3-/4-}$ as a redox probe.

Despite the numerous advantages of aptamers, they still suffer from some limitations. As they are nucleic acid biopolymers, the in situ application of aptamers are crucially limited by their inherent physicochemical characteristics. For overcoming that, various analytical parameters should be considered and predetermined during the selection procedure of aptamers. Therefore, choosing the optimum incubation time and

Table 1 Comparison between analytical performance of this method and other reported techniques for detection of myoglobin

Electrode and sensor	Technique	LOD	Linear range	Refs.
Mb-aptamer-Au electrode	Chronocoulometry	10.0 pM	10.0 pM-100 nM	[24]
PLL[1]-BP[2]-Apt-modified electrodes	Cyclic Voltammetry	0.031 pM	0.05 pM-0.95 μM	[25]
aptamer/PG[3]/SNPs[4]-Streptavidin	Fluorescence	52.0 pM	0.13 nM- 45.0 nM	[26]
aptamer /rGO[5]/CNT [6]/SPE[7]	Cyclic Voltammetry	20.0 pM	59.0 pM-239 nM	[27]
CS[8]/SPGEs[9]	Differential Pulse Voltammetry	27.0 pM	100 pM- 40.0 nM	[28]
RGD[10]/GR-COOH[11]/GCE[12]	Differential Pulse Voltammetry	1.57 nM	5.90 μM-11.9 mM	[29]
poly-o-PD[13]/MIP[14] sensor	Square Wave Voltammetry	0.50 nM	1.00 nM-1.00 μM	[30]
PGM[15] sensor	Surface Plasmon Resonance	50.0 pM	50.0 pM-200 nM	[31]
AuNPs/WS$_2$ nanohybrid	Single molecule Surface Enhanced Raman Scattering	0.50 fM	0.50 fM – 5.00 pM	[32]
rGO/ Ru(bpy)$_3$$^{2+}$ [16]/ Sm$_2$O$_3$NPs/ SPCE[17]	Electrochemiluminescence	12.0 pM	0.05 nM - 25.0 nM	[33]
MIP/CNT/GCE	Cyclic Voltammetry	9.70 nM	60.0 nM −6.00 μM	[34]
AuNPs /rGO/ SPE	Differential Pulse Voltammetry	52.0 μM	78.0 μM – 110 nM	[35]
This work	Differential Pulse Voltammetry	2.20 pM	0.01–1.00 nM and 10.0 nM–200 nM	–

1: Poly- L-lysine (PLL), 2: Black phosphorus nanosheets, 3: Pico green, 4: Silica nanoparticles, 5: Reduced graphen oxide, 6: Carbon nanotube, 7: Screen printed electrodes, 8: Dual-aptamer (DApt)-complementary strand of aptamer (CS), 9: Screen-printed gold electrodes (SPGEs), 10: Arginine-glycine-aspartic, 11: Carboxylated graphene, 12: Glassy carbon electrode, 13: Poly-o-phenylenediamine, 14: Molecularly imprinted polymer, 15: Personal glucose meter, 16: Ruthenium(II)-tris(2,2- bipyridyl), 17: Screen-printed carbon electrode
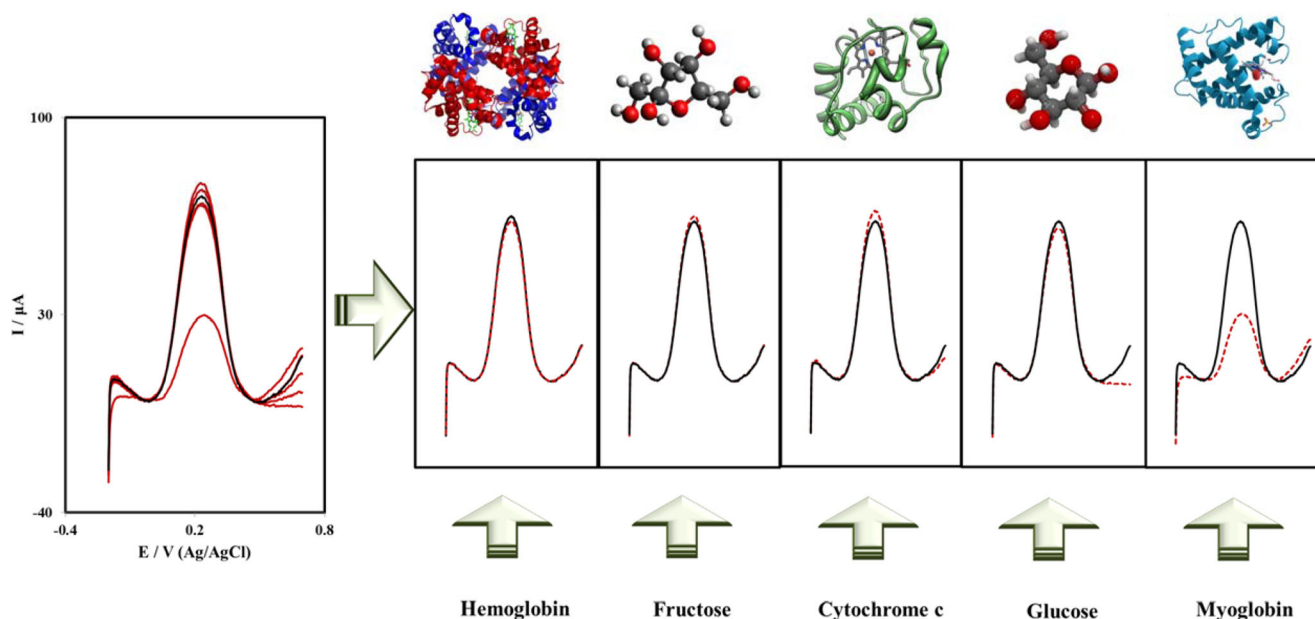
Fig. 6 DPV responses of prepared aptasensor before (solid line) and after (dashed line) being incubated in the solution containing 50 μM hemoglobin, fructose, cytochrome c, and glucose, and 50 nM Mb recorded in solution containing 5.0 mM $[Fe(CN)_6]^{3-/4-}$ and 0.1 M phosphate buffer. Condition: modulation amplitude: 0.05 V, pulse width: 0.05 s, sample width: 0.0167 s, step potential of 0.001 mV, working voltage: 0.2 V vs. Ag/AgCl

optimum concentration of Mb-aptamer were considered as limitation for this experimental. According to our results, 0.5 μM and 30 min were obtained as optimum aptamer concentration and optimum incubation time, respectively. Non-specific interaction of analyte as a major drawback was overcome utilizing high ionic strength solution. Also, steric hindrance caused by too close proximity of aptamer and surface have been overcome by introduction of 5'-NH_2-$(CH_2)_6$ group as spacer molecules which produce additional space for proper aptamer folding. Under the optimum condition the detection limit for Mb was calculated as low as 2.2 ± 0.1 pM, at concentration range up to 200 nM.

Compliance with ethical standards The author(s) declare that they have no competing interests.

Fig. 7 Stability of the aptamer/PtSnNP/CNT/GCE tested by 50 repetitive potential sweeps in the solution containing 5.0 mM $[Fe(CN)_6]^{3-/4-}$ and 0.1 M phosphate buffer. Condition: scan rate: 50 mV s^{-1}, sweeping potential: −0.6 V and 0.8 V

References

1. Zhu J, Zou N, Mao H, Wang P, Zhu D, Ji H, Cong H, Sun C, Wang H, Zhang F, Qian J, Jin Q, Zhao J (2013) Evaluation of a modified lateral flow immunoassay for detection of high-sensitivity cardiac troponin I and myoglobin. Biosens Bioelectron 42:522–525
2. W H O World Health Statistics 2014, http://www.who.int/gho/publications/world-health-statistics/2014/en, (accessed May 12, 2016)
3. Nambi V, Liu X, Chambless LE, de Lemos JA, Virani SS, Agarwal S, Boerwinkle E, Hoogeveen RC, Aguilar D, Astor BC, Srinivas PR, Deswal A, Mosley TH, Coresh J, Folsom AR, Heiss G, Ballantyne CM (2013) Troponin T and N-terminal pro-B-type natriuretic peptide: a biomarker approach to predict heart failure risk-the atherosclerosis risk in communities study. Clin Chem 59:1802–1810
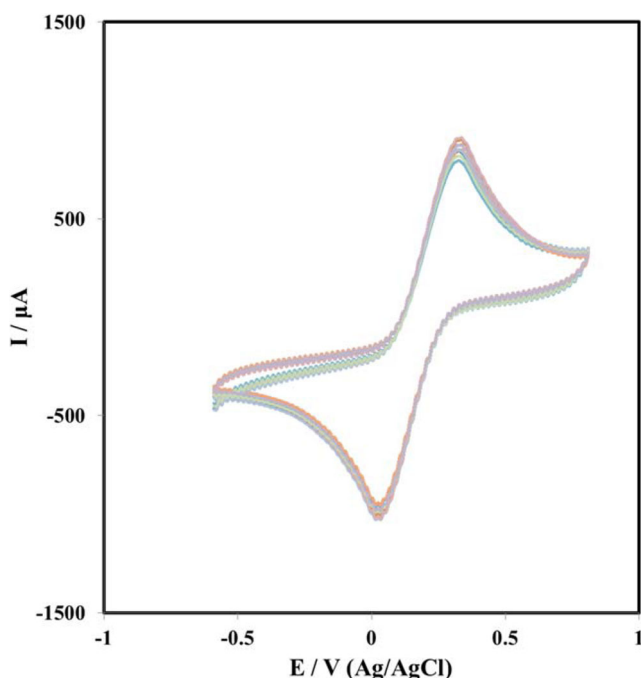4. Aldous SJ (2013) Cardiac biomarkers in acute myocardial infarction. Int J Cardiol 164:282–294

5. Pervaiz S, Anderson FP, Lohman TP, Lawson CJ, Feng YJ, Waskiewicz D (1997) Comparative analysis of cardiac troponin I and creatine kinase-MB as markers of acute myocardial infarction. Clin Cardiol 20:269–271

6. Janota T (2014) Biochemical markers in the diagnosis of myocardial infarction. Cor Vasa 56: e304–e310

7. Stone MJ, Waterman MR, Harimoto D, Murray G, Willson N, Platt MR, Blomqvist G, Willerson JT (1997) Serum myoglobin level as diagnostic test in patients with acute myocardial infarction. Br Heart J 39:375–380

8. Kumar V, Shorie M, Ganguli AK, Sabherwal P (2015) Graphene-CNT nanohybrid aptasensor for label free detection of cardiac biomarker myoglobin. Biosens Bioelectron 72:56–60

9. Li YC, Li YJ, Yang YY (2011) Direct electrochemistry and electrocatalysis of myoglobin-based nanocomposite membrane electrode. Bioelectrochemistry 82:112–116

10. Naveena BM, Faustman C, Tatiyaborworntham N, Yin S, Ramanathan R, Mancini RA (2010) Detection of 4-hydroxy-2-nonenal adducts of turkey and chicken myoglobins using mass spectrometry. Food Chem 122:836–840

11. Giaretta N, Giuseppe AM, Lippert M, Parente A, Maro AD (2013) Myoglobin as marker in meat adulteration: A UPLC method for determining the presence of pork meat in raw beef burger. Food Chem 141:1814–1820

12. Yue Q, Song Z (2006) Assay of femtogram level nitrite in human urine using luminol–myoglobin chemiluminescence. Microchem J 84:10–13

13. Zhang X, Kong X, Fan W, Du X (2011) Iminodiacetic acid-functionalized gold nanoparticles for optical sensing of myoglobin via Cu^{2+} coordination. Langmuir 27:6504–6510

14. Gnedenko OV, Mezentsev YV, Molnar AA, Lisitsa AV, Ivanov AS, Archakov AI (2013) Highly sensitive detection of human cardiac myoglobin using a reverse sandwich immunoassay with a gold nanoparticle-enhanced surface plasmon resonance biosensor. Anal Chim Acta 759:105–109

15. Yang Z, Zhou DM (2006) Cardiac markers and their point-of-care testing for diagnosis of acute myocardial infarction. Clin Biochem 39:771–780

16. Ellington AD, Szostak JW (1990) In vitro selection of RNA molecules that bind specific ligands. Nature 346:818–822

17. Famulok M, Mayer G (2011) Aptamer modules as sensors and detectors. Acc Chem Res 44:1349–1358

18. Sabherwal P, Mutreja R, Suri CR (2016) Biofunctionalized carbon composites: new-generation diagnostic tools. TrAC Trends Anal Chem 82:12–21

19. Holzinger M, Goff AL, Cosnier S (2014) Nanomaterials for biosensing applications: a review. Front Chem 2:1–10

20. Britz DA, Khlobystov AN (2006) Noncovalent interactions of molecules with single walled carbon nanotubes. Chem Soc Rev 35:637–659

21. Wang J, Liu G, Jan MR (2014) Ultrasensitive electrical biosensing of proteins and DNA: carbon-nanotube derived amplification of the recognition and transduction Eevents. J Am Chem Soc 126:3010–3011

22. Li H, Chen S, Li Q, Liu F (2016) Effect of the pH of the preparation medium on the microstructure and electrocatalytic activity of carbon nanotubes decorated with PtSn nanoparticles for use in methanol oxidation. New Carbon Mater 31:293–300

23. Christina B, Chantal P, Martin C (2004) Size-selected synthesis of PtRu nano-catalysts: reaction and size control mechanism. J Am Chem Soc 126:8028–8037

24. Wang Q, Liu W, Xing Y, Yang X, Wang K, Jiang R, Wang P, Zhao Q (2014) Screening of DNA aptamers against myoglobin using a positive and negative selection units integrated microfluidic chip and its biosensing application. Anal Chem 86:6572–6579

25. Kumar V, Brent JR, Shorie M, Kaur H, Chadha G, Thomas AG, Lewis EA, Rooney AP, Nguyen L, Zhong XL, Burke MG, Haigh SJ, Walton A, McNaughter PD, Tedstone AA, Savjani N, Muryn CA, Brien P, Ganguli AK, Lewis DJ, Sabherwal P (2016) Nanostructured aptamer-functionalized black phosphorus sensing platform for label-free detection of myoglobin, a cardiovascular disease biomarker. ACS Appl Mater Interfaces 8:22860–22868

26. Abnous K, Danesh NM, Emrani AS, Ramezani M, Taghdisi SM (2016) A novel fluorescent aptasensor based on silica nanoparticles, PicoGreen and exonuclease III as a signal amplification method for ultrasensitive detection of myoglobin. Anal Chim Acta 917:71–78

27. Kumar V, Shorie M, Ganguli AK, Sabherwal P (2015) Graphene-CNT nanohybrid aptasensor for label free detection of car- diac biomarker myoglobin. Biosens Bioelectron 72:56–60

28. Taghdisi SM, Danesh NM, Ramezani M, Emrani AS, Abnous K (2016) A novel electrochemical aptasensor based on Y-shape structure of dual-aptamer-complementary strand conjugate for ultrasensitive detection of myoglobin. Biosens Bioelectron 80:532–537

29. Li C, Li J, Yang X, Gao L, Jing L, Ma X (2017) A label-free electrochemical aptasensor for sensitive myoglobin detection in meat. Sensors Actuators B Chem 242:1239–1245

30. Shumyantseva VV, Bulko TV, Sigolaeva LV, Kuzikov AV, Archakov AI (2016) Electrosynthesis and binding properties of molecularly imprinted poly-o-phenylenediamine for selective recognition and direct electrochemical detection of myoglobin. Biosens Bioelectron 86:330–336

31. Wang Q, Liu F, Yang X, Wang K, Wang H, Deng X (2015) Sensitive point-of-care monitoring of cardiac biomarker myoglobin using aptamer and ubiquitous personal glucose meter. Biosens Bioelectron 64:161–164

32. Shorie M, Kumar V, Kaur H, Singh K, Tomer VK, Sabherwal P (2018) Plasmonic DNA hotspots made from tungsten disulfide nanosheets and gold nanoparticles for ultrasensitive aptamer-based SERS detection of myoglobin. Microchim Acta 185:158

33. Karimi Pur MR, Hosseini M, Faridbod F, Ganjali MR (2017) Highly sensitive label-free electrochemiluminescence aptasensor for early detection of myoglobin, a biomarker for myocardial infarction. Microchim Acta 184:3529–3537

34. Wang Y, Han M, Ye X, Wu K, Wu T, Chunya Li C (2017) Voltammetric myoglobin sensor based on a glassy carbon electrode modified with a composite film consisting of carbon nanotubes and a molecularly imprinted polymerized ionic liquid. Microchim Acta 184:195–202

35. Singh S, Tuteja SK, Sillu D, Deep A, Suri CR (2016) Gold nanoparticles-reduced graphene oxide based electrochemical immunosensor for the cardiac biomarker myoglobin. Microchim Acta 183:1729–1738